Journal of Applied Physics

Bayesian-optimized infrared grating for tailoring thermal emission to boost thermophotovoltaic performance

Cite as: J. Appl. Phys. **133**, 124904 (2023); https://doi.org/10.1063/5.0138747
Submitted: 14 December 2022 • Accepted: 11 March 2023 • Published Online: 29 March 2023

Yiting Zhao, Fan Yang, Jinlin Song, et al.

AIP Publishing

Journal of Applied Physics ARTICLE scitation.org/journal/jap

Bayesian-optimized infrared grating for tailoring thermal emission to boost thermophotovoltaic performance

Cite as: J. Appl. Phys. **133**, 124904 (2023); doi: 10.1063/5.0138747
Submitted: 14 December 2022 · Accepted: 11 March 2023 ·
Published Online: 29 March 2023

Yiting Zhao,[1] Fan Yang,[1] Jinlin Song,[2,a)] and Run Hu[1,3,a)]

AFFILIATIONS

[1]China-EU Institute for Clean and Renewable Energy, Huazhong University of Science and Technology, Wuhan 430074, China
[2]School of Electrical and Information Engineering, Wuhan Institute of Technology, Wuhan 430205, China
[3]School of Energy and Power Engineering, Huazhong University of Science and Technology, Wuhan 430074, China

[a)]**Authors to whom correspondence should be addressed:** songjinlin@wit.edu.cn and hurun@hust.edu.cn

ABSTRACT

Thermophotovoltaic (TPV) devices, which can break the Shockley–Queisser limit (33.7%) and enhance the thermal energy utilization efficiency, have garnered increasing attention in recent decades. Structuring the emitter surface has been demonstrated to be powerful for tailoring thermal emission to enhance the power density and system efficiency of a TPV system. However, the design and optimization of the broad parameters of the surface nanostructures manually remain to be thorny issues. In this paper, the Bayesian algorithm under the framework of material informatics was coupled with a rigorous coupled wave analysis to optimize the geometry of the infrared grating nanostructure to achieve wavelength-selective emission to boost the TPV performance. It is demonstrated that only less than 0.173% of the total candidate structures were calculated to find out the optimal structure with high spectral emittance in the range of 0.3–1.708 μm, and the power density and system efficiency of the TPV system were enhanced to 4.20 W/cm^2 and 35.37%, respectively. The present machine-learning-based optimization of a multi-parameter nanostructure can improve the performance of the TPV system significantly and can be extended to other physical fields in a feasible manner.

I. INTRODUCTION

Thermophotovoltaic (TPV) devices are able to directly convert radiant thermal energy from emitters into electric power via TPV cells with high output power and conversion efficiency;[1,2] thus, they have been proposed to broaden the application scenarios beyond solar light like hybrid vehicles,[3] deep space exploration,[4] aggregated photovoltaics,[5] and thermal energy storage.[6,7] The principle of the TPV system is similar to the traditional solar photovoltaic (PV) system, except that they differ in the conversion spectrum, as the solar PV system converts the solar spectrum while the TPV system mainly converts the infrared band of the thermal radiation spectrum. The high-energy photons emitted from the emitter excite electron leaps in the cell, and such carriers are subsequently separated and extracted as electricity.[8] To solve the spectral mismatch between emitters and TPV cells, most TPV systems adopt selective emitters to tailor thermal radiation and effectively reduce the heat loss in a TPV cell. However, despite many decades of research, it is still a challenge to achieve perfect spectral selectivity of TPV emitters.

In the design of selective TPV emitters, machine learning algorithms have been used to optimize selective emitters, such as genetic algorithms,[9] adversarial autoencoder networks,[10] and particle swarm optimization.[11] However, due to the huge number of candidates for selective emitters, these methods are either costly or time-consuming. Zhang *et al.* employed the Bayesian optimization method to design the highly wavelength-selective, aperiodic multilayer TPV emitters and verified that Bayesian optimization is effective in designing selective emitters.[12] To achieve wavelength-selective emitters, nanostructures such as grating,[13,14] photonic crystals,[15,16] and metamaterials[17,18] in all dimensional domains have been extensively investigated. The incident wave interacts with the nanostructure to excite various kinds of resonances, like surface plasmon polaritons (SPPs),[19] magnetic polaritons (MPs),[20] surface

phonon polaritons (SPhPs),[21] Tamm plasmon,[22] and micro-cavity resonance,[23] thereby achieving significantly strong thermal emission at certain wavelengths.[24] Jeon *et al.* optimized one-dimensional TiO_2/SiO_2 photonic crystals to get the Pareto front of the power density and system efficiency of a TPV system, but they neglected the intrinsic photo-to-current characteristics of the TPV cells.[25] Hu *et al.* further applied materials informatics combined with the detailed balance analysis of the TPV cells to design a Tamm emitter.[26] These one-dimensional photonic crystals can be optimized, but the design space is limited as design parameters are the material's thickness and configuration. Beyond the photonic crystals, people also designed the nanostructure grating for TPV emitters. Wang *et al.* proposed a wavelength-selective and diffuse TPV emitter made of tungsten gratings with a SiO_2 dielectric layer by manually zeroing the total impedance.[20] Nguyen-Huu *et al.* combined rigorous coupled-wave analysis (RCWA) and genetic algorithm to tailor the tungsten grating for a wavelength-selective but polarization-insensitive TPV emitter.[27] Regrettably, these studies did not couple the emitter with TPV cells, thus failed to guarantee that the optimized emitter matched with the TPV cell to boost the whole performance.

In this study, we employ the Bayesian algorithm to optimize the one-dimensional nanostructure with infrared tungsten gratings and SiO_2 dielectric layer, as a direction-insensitive selective emitter, to boost the output power density and system efficiency of a single-junction GaSb cell in the TPV system. What is more, the spectral emittance and electromagnetic field distributions of the optimized selective emitter are calculated to confirm the physical mechanisms and compare them with the selective emitter that is manually optimized.

II. METHODOLOGY

In the TPV system, the wavelength-selective emitter is composed of a tungsten grating on a SiO_2 dielectric layer and a tungsten substrate in sequence, thus constituting the metal–insulator–metal (MIM) nanostructure. Tungsten is chosen as the material for gratings and substrates owing to its high thermal conductivity, high refractory properties, and being highly lossy in the near-infrared. The structure of the selective emitter is represented by the period (Γ), the filling factor (f), the thickness of gratings (d_1), and the thickness of the SiO_2 layer (d_2). The surface absorptance (α) or emittance (ε) can be assumed as equal due to Kirchhoff's law and can be determined by a rigorous coupled-wave analysis (RCWA) method in our interested wavelength range of 0.3–5.0 μm.[28] As transverse electric (TE) waves cannot excite MPs, only the transverse magnetic (TM) waves are considered hereinafter.[29,30] GaSb has a bandgap of 0.726 eV (1.708 μm)[31] which lies in the infrared range and is easy to realize. According to Wien's law, the temperature of the selective emitter should be $T_e = 1700$ K to guarantee the peak wavelength above the bandgap energy. By comparison, a higher bandgap requires a higher emitter temperature, and a cell having a lower bandgap is of high cost. Furthermore, considering the excellent external quantum efficiency (EQE) at infrared wavelengths, we select the GaSb cell to convert thermal photons emitted by the emitter to electricity in this work.

Figure 1 displays the flow chart for design and optimization of the selective emitter of the TPV system. The COMmon Bayesian Optimization Library (COMBO), an efficient Bayesian optimization protocol based on a machine-learning kernel, was adopted to optimize the structure of the selective emitter, and an open-source package is used throughout the optimization process.[32] It is an efficient Bayesian optimization protocol based on a machine-learning kernel, and it employs Thompson sampling, random feature maps, one-rank Cholesky update, and automatic hyperparameter tuning. Meanwhile, as a Python package, it will be easily combined with other materials informatics packages and is more pervasive. The optimization process is mainly composed of four parts: descriptors, an optimization method, a calculation tool, and an evaluation criterion.[14] In the optimization process, we first prepare the candidate pool by permutation and combination of parameters of infrared gratings. This gives rise to 2.96×10^6 possible candidate structures. Then we randomly select 20 candidates as initial structures and calculate the corresponding figure of merit (FOM) value to estimate the initial prediction model. The model starts from an *a priori* hypothesis, iteratively increases the amount of prior information, and modifies the prior model to obtain a more accurate surrogate model. Here, because of the competition between P_{out} and η, FOM can be denoted by

$$\mathrm{FOM} = P_{out} \times \eta. \tag{1}$$

For the TPV cell, the maximum output power per unit area can be calculated as

$$P_{\mathrm{out}} = V_{\mathrm{oc}} J_{\mathrm{sc}} \varphi_{\mathrm{FF}}, \tag{2}$$

where J_{sc} is the short circuit current density, V_{oc} is the open circuit voltage, and φ_{FF} is the fill factor. For an ideal TPV cell, Shockley and Queisser indicated that the current–voltage relationship is given by[33]

$$J(V) = J_{\mathrm{sc}} - J_0 \left[\exp\left(\frac{qV}{k_{\mathrm{b}} T_{\mathrm{c}}} \right) - 1 \right], \tag{3}$$

where q is the elementary charge and k_b is the Boltzmann constant. J_0 is the sum of the reverse-saturation current of the P–N junction, which can be calculated as[34]

$$J_0 = \beta T_{\mathrm{c}}^3 \exp\left(-\frac{E_{\mathrm{g}}}{k_{\mathrm{b}} T_{\mathrm{c}}} \right), \tag{4}$$

where β equals $3.165 \times 10^{-4} \exp(2.915 \times E_g)$ that combines all the dimensional, doping, and minority carrier transport parameters for a TPV cell and is determined by obtaining the best fit between modeled cell performance and actual measured performance for single-junction cells.[34] The open-circuit voltage (V_{oc}) results from solving Eq. (2) for $J = 0$ are

$$V_{\mathrm{oc}} = \frac{k_{\mathrm{b}} T_{\mathrm{c}}}{q} \ln\left(\frac{J_{\mathrm{sc}}}{J_0} + 1 \right). \tag{5}$$

The photocurrent generated by the TPV cell is not only related to the photon number density above the bandgap but also proportional to the external quantum efficiency of the TPV cell. The

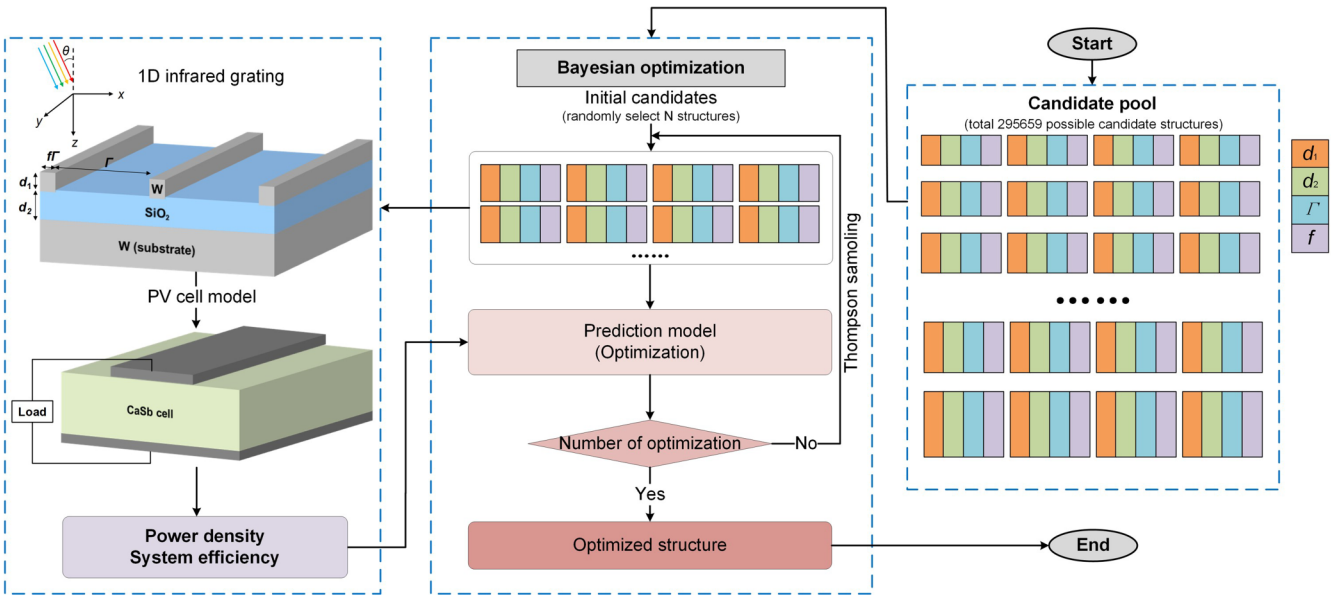

FIG. 1. Roadmap of machine-learning Bayesian algorithm optimization.

short-circuit current J_{sc} can be obtained by integrating the photocurrent generated by the TPV cell at different wavelengths as[35]

$$J_{sc} = q\int_{\lambda_0}^{\lambda_g} \frac{I_{BB}\varepsilon_R(\lambda)\eta_{EQE}(\lambda)d\lambda}{hc_0/\lambda}, \tag{6}$$

where I_{BB} is the blackbody spectral density, λ_0 is the lower wavelength of the incident spectrum (0.3 μm), $\varepsilon_R(\lambda)$ is the spectral emittance of the selective emitter calculated by RCWA, c_0 is the speed of light in vacuum, and η_{EQE} is the wavelength-dependent quantum efficiency of the GaSb cell.[35] The filling factor (φ_{FF}) in Eq. (1) can be expressed as[36]

$$\varphi_{FF} = \frac{V^* - \ln(V^* - E_g)}{V^* + 1}, \tag{7}$$

where V^* is expressed as the normalized open circuit voltage,

$$V^* = \frac{q}{k_b T_c} V_{oc}. \tag{8}$$

According to Planck's law, the incident photon energy from the selective emitter is

$$P_{rad} = \int_{\lambda_0}^{\lambda_1} I_{BB}\varepsilon_R(\lambda)d\lambda, \tag{9}$$

where λ_1 is the upper wavelength of the incident spectrum (5 μm). Here, the efficiency (η) of the TPV system is defined as the ratio of the output power density (P_{out}) of the system to the incident radiation energy of the GaSb cell (P_{rad}).

Based on the initial prediction model, Thompson sampling enables the next candidates to be selected according to the probability of being optimum. Then, another round of Bayesian optimization is conducted and the prediction model is updated. By repeating this procedure, the optimized structure can be found quickly.

III. RESULTS AND DISCUSSION

As shown in Fig. 2(a), the system efficiency and power density of all calculated candidates in the optimization process are plotted in gray dots. We also plot the Pareto front curve to find the global optimum structures, shown as blue circles, and the red dot denotes the global optimum case.[26] It can be seen that through the COMBO algorithm using the quantum efficiency of the GaSb cell as a function of wavelength [see Fig. 2(c)],[35] the corresponding parameters of the optimal selective emitters are $d_1 = 0.026\,\mu$m, $d_2 = 0.1\,\mu$m, $\Gamma = 0.35\,\mu$m, $f = 0.6$, $P_{out} = 4.2$ W/cm^2, and $\eta = 35.4\%$, which surpass the Shockley–Queisser limit of 33.7%. We compare the case with a thin-film emitter (black square, $d_1 = 0.026\,\mu$m, $d_2 = 0.1\,\mu$m) to represent the superiority of the optimal optimization result. Furthermore, by tracing the largest FOM in Fig. 2(b), we found that only a small number of structures (511/2 956 659 = 0.173%) were calculated to find the global optimum structure, validating the high efficiency of the present Bayesian optimization algorithm. Figure 2(c) shows the quantum efficiency of the GaSb cell as a function of wavelength.[35]

After that, we compare the emission characteristics of the optimum selective emitter with the thin-film emitter and the

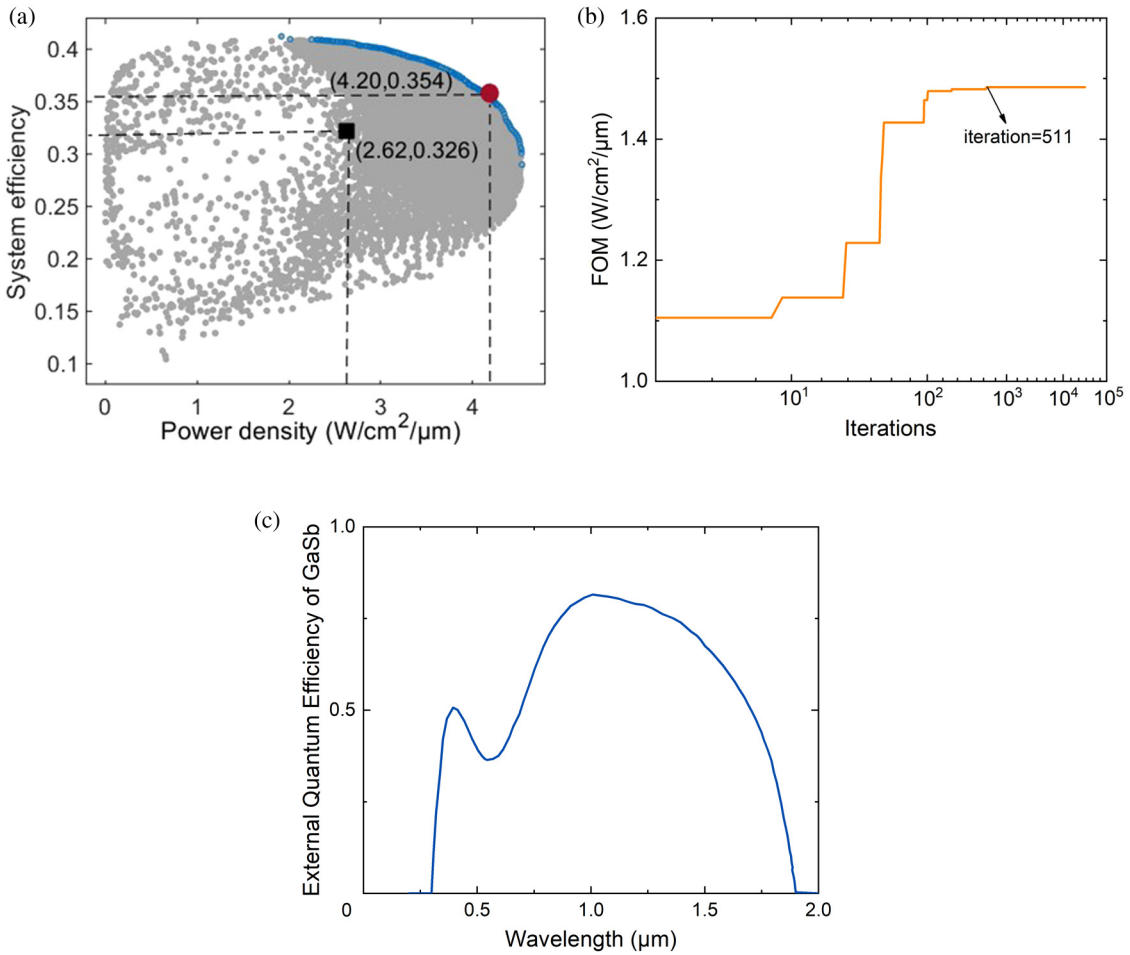

FIG. 2. (a) P_{out} and η of the selective emitter optimized by the Bayesian algorithm; (b) the iterative process of Bayesian algorithm optimization; and (c) quantum efficiency of a GaSb cell vs wavelength.

selective emitter of Wang *et al.* for TM and TE waves as in Figs. 3(a) and 3(b).[20] As we know, the emission spectrum of an ideal selective emitter should only emit photons that are exactly equal to E_g since the excess energy does not contribute to the efficiency of the battery. According to the simulation results, it can be obtained that the surface nanostructures can enhance the radiation performance of the emitter. Moreover, the optimal selective emitter with IR grating shows the highest emissivity around λ_g and maintains a high emissivity at shorter wavelengths that can be absorbed by the TPV cell, while the emissivity starts to decrease at very short wavelengths (ultra-high energy photons), avoiding the excess photon energy from heating the TPV cell and reducing the efficiency of the TPV cell. In addition, the performance of the emitter under TM waves is enhanced more significantly, which verifies that 1D gratings cannot excite MPs under TE waves.

To clearly evaluate the wavelength selectivity of the optimum selective emitter optimized by the Bayesian algorithm, we adopt the calculation of suppression (S) of emittance proposed by Sakib *et al.* for TM waves,[37]

$$S = 10\log\frac{1}{\varepsilon}. \tag{10}$$

As shown in Fig. 3(c), the emittance of the optimum selective emitter demonstrates better suppression than that of the thin-film emitter and the emitter in Ref. 20 in the undesired emission range, while in the desired emission range, the suppression effect is reversed. Besides, we also compare the J–V curves of the TPV systems with different selective emitters in Fig. 3(d). It is found that the photocurrent of the optimized TPV system is significantly improved since the spectrum of the optimum selective emitter exhibits a higher emittance in the range of 0.3–1.708 μm and less thermal emission above the bandgap wavelength (λ_g). Thus, the TPV cell absorbs more photons above the bandgap energy, and the

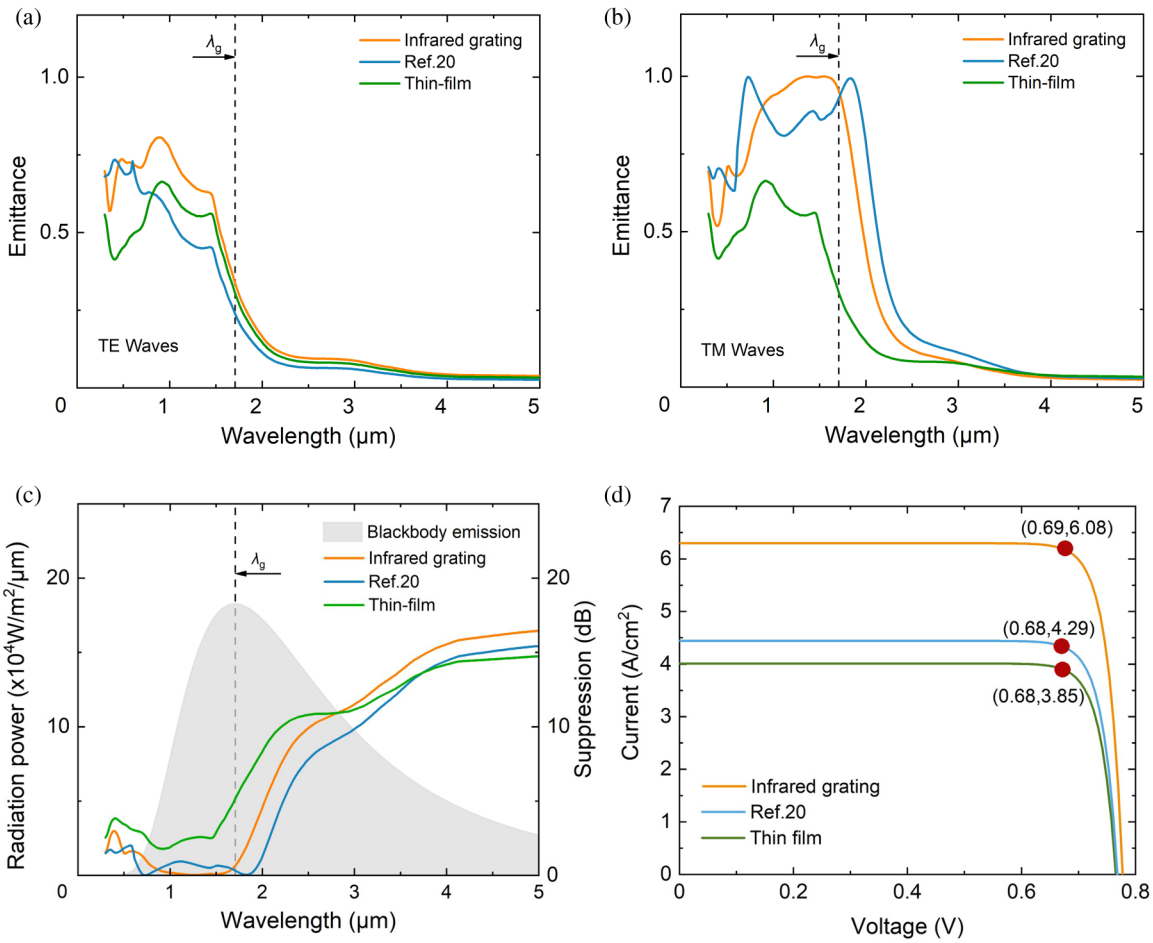

FIG. 3. Comparison of the emission characteristics of the selective emitter based on the optimum structure, the thin-film emitter, and the emitter in Ref. 20. (a) and (b) Normal emission spectra (TE waves and TM waves); (c) emittance and suppression and (d) J–V curves.

photocurrent will increase, which is closely connected to the selectivity of thermal radiation by the emitter optimized by the Bayesian algorithm.

Another important feature of the infrared grating selective emitter is the directional insensitivity of the emission peaks. As shown in Fig. 4(a), the efficiency of the TPV system is barely affected by θ and can be maximized all the time. To explain the physical mechanism of the feature, we investigated the internal relationship among λ, θ, and ε. Figure 4(b) shows the contour plot of the emittance for the infrared grating selective emitter at TM waves in terms of λ and θ. It is evident that the emittance value remains high ($\varepsilon > 0.8$) for θ shorter wavelength up to 80° and begins to drop beyond 1.708 μm. Furthermore, there are two bright bands that indicate emittance peaks in Fig. 4(b), which suggest that the wavelength range of the two bands is wide, indicating that the emittance of the selective emitter with optimum structure parameters continues to maintain a high value within the desired range of the emission spectrum. The first bright band near 1.708 μm is excited by MPs and we can find that the bright band does not tilt as θ increases, since the MP resonance frequency is insensitive to θ as long as the magnetic field is along the grating grooves.[38] It is seen that the magnetic field is strongly enhanced in the SiO_2 dielectric layer inserted between tungsten gratings and the tungsten substrate, which can be explained by the excitation of MPs.[39] MPs consist of magnetically excited LC-resonance between the two coupled metallic layers and the electric response of metal gratings to external incident waves.[40] The equivalent LC circuit model predicts that the resonance frequency of MPs mostly depends on the geometric parameters of the nanostructure and the properties of materials for the infrared grating nanostructure.[33] According to Lenz's law, an anti-parallel current (as indicated by arrows) at the surface of tungsten gratings can be obtained in the y direction of the incident wave with the time-varying magnetic field, and the anti-parallel current can introduce antimagnetic resonance coupled with incident electromagnetic waves, which ultimately enhances the emittance of the desired spectral region. The other bright band at a

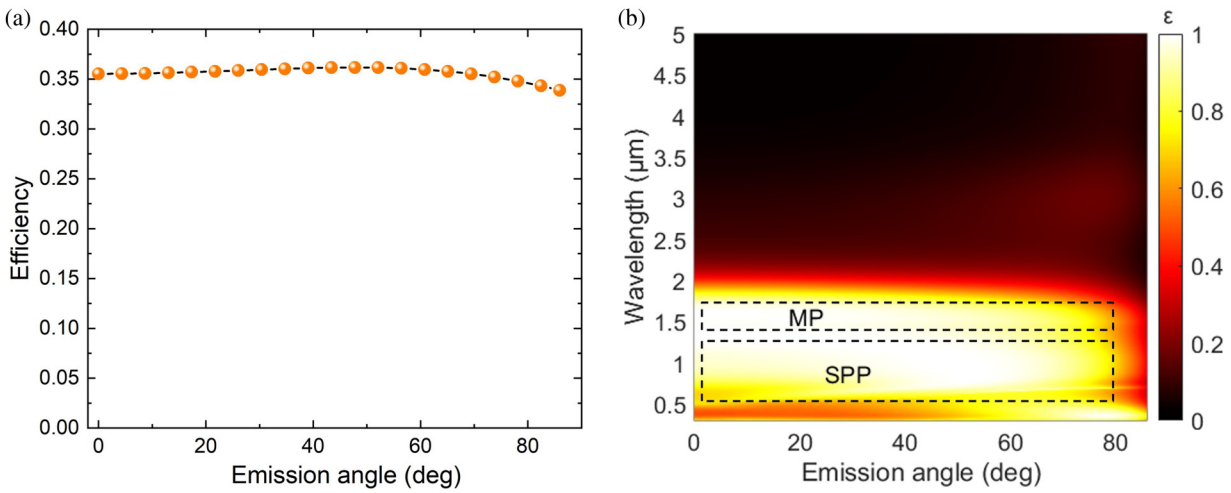

FIG. 4. Directional insensitivity and the physical mechanism of the optimized selective emitter. (a) The efficiency of the optimized TPV system at different emission angles (θ) for TM waves. (b) Contour plots of emittance of the optimized TPV emitter as a function of wavelength and emission angle (θ).

range of the shorter wavelength excited by SPPs is little inclined. SPPs are strong coupling of the incident wave with collective charge density oscillations on the periodic infrared grating structure. The stimulated SPPs capture most of the incident photons and reemit them in the forward direction, thus having a high transmittance at certain wavelengths. The transmission capabilities can be controlled by tuning the grating parameters. Compared with the results of Wang *et al.*, the SPPs direction dependence of the selective emitter optimized by the Bayesian algorithm is significantly reduced.[20] Thus, the direction sensitivity of the SPPs can be reduced by adjusting the geometric parameters of the selective emitter.

IV. CONCLUSIONS

In summary, based on the combination of Bayesian algorithm optimization and the RCWA method, we modulate the wavelength-selective infrared emitter to boost TPV performance by exciting SPPs and MPs. The Pareto front lines of the power density and system efficiency are obtained for the infrared grating selective emitter. It is demonstrated that the emitter based on the MIM nanostructure with infrared gratings can achieve a higher emittance and directional insensitivity in the desired spectral region, suppress the thermal emission above the bandgap wavelength, and match to the GaSb cell better than the thin-film emitter, thus boosting the output power density (4.2 W/cm^2) and system efficiency (35.4%) simultaneously. Moreover, the maximum FOM could be realized within calculations for less than 0.173% of the total candidate structures, which is more efficient than other machine-learning algorithms. The present machine-learning optimization framework can be extended for black-box global optimization problems in other fields beyond the TPV system.

ACKNOWLEDGMENTS

The authors acknowledge the financial support from the National Natural Science Foundation of China (NNSFC) (Nos. 52211540005 and 52076087), the Wuhan City Science and Technology Program (No. 2020010601012197), and Wuhan Knowledge Innovation Program, and Startup Program at Wuhan Institute of Technology (No. K2021026).

AUTHOR DECLARATIONS

Conflict of Interest

The authors have no conflicts to disclose.

Author Contributions

Yiting Zhao: Validation (lead); Visualization (lead); Writing – original draft (lead). **Fan Yang:** Data curation (equal); Validation (equal). **Jinlin Song:** Funding acquisition (equal); Methodology (equal); Supervision (equal); Writing – review & editing (equal). **Run Hu:** Conceptualization (lead); Funding acquisition (equal); Methodology (equal); Supervision (equal); Writing – review & editing (equal).

DATA AVAILABILITY

The data that support the findings of this study are available from the corresponding authors upon reasonable request.

REFERENCES

[1]A. Waske, D. Dzekan, K. Sellschopp, D. Berger, A. Stork, K. Nielsch, and S. Fähler, Nat. Energy **4**(1), 68 (2019).
[2]X. Shi and J. He, Science **371**(6527), 343 (2021).
[3]G. Colangelo, A. de Risi, and D. Laforgia, Semicond. Sci. Technol. **18**(5), S262 (2003).

[4]A. Datas and A. Martí, Sol. Energy Mater. Sol. Cells **161**, 285 (2017).
[5]Y. Tavakol-Moghaddam, Y. Saboohi, and A. Fathi, Renew. Energy **190**, 78 (2022).
[6]C. Amy, H. R. Seyf, M. A. Steiner, D. J. Friedman, and A. Henry, Energy Environ. Sci. **12**(1), 334 (2019).
[7]A. Lenert, D. M. Bierman, Y. Nam, W. R. Chan, I. Celanovic, M. Soljacic, and E. N. Wang, Nat. Nanotechnol. **9**(2), 126 (2014).
[8]D. Fan, T. Burger, S. McSherry, B. Lee, A. Lenert, and S. R. Forrest, Nature **586**(7828), 237 (2020).
[9]N. Jeon, D. J. Mandia, S. K. Gray, J. J. Foley, and A. B. F. Martinson, ACS Appl. Mater. Interfaces **11**(44), 41347 (2019).
[10]Z. A. Kudyshev, A. V. Kildishev, V. M. Shalaev, and A. Boltasseva, Nanophotonics **10**(1), 371 (2020).
[11]H. Wang, H. Alshehri, H. Su, and L. P. Wang, Sol. Energy Mater. Sol. Cells **174**, 445 (2018).
[12]W. B. Zhang, B. X. Wang, and C. Y. Zhao, ACS Appl. Energy Mater. **4**(2), 2004 (2021).
[13]H. T. Yu, D. Liu, Z. Yang, and Y. Y. Duan, Sci. Rep. **7**(1), 1026 (2017).
[14]B. Zhao, L. P. Wang, Y. Shuai, and Z. M. M. Zhang, Int. J. Heat Mass Transfer **67**, 637–645 (2013).
[15]D. M. Bierman, A. Lenert, W. R. Chan, B. Bhatia, I. Celanović, M. Soljačić, and E. N. Wang, Nat. Energy **1**, 16068 (2016).
[16]K. A. Arpin, M. D. Losego, A. N. Cloud, H. Ning, J. Mallek, N. P. Sergeant, L. Zhu, Z. Yu, B. Kalanyan, G. N. Parsons, G. S. Girolami, J. R. Abelson, S. Fan, and P. V. Braun, Nat. Commun. **4**, 2630 (2013).
[17]R. Hu, W. Xi, Y. Liu, K. Tang, J. Song, X. Luo, J. Wu, and C.-W. Qiu, Mater **45**, 120–141 (2021).
[18]J. L. Song, S. Y. Huang, Y. P. Ma, Q. Cheng, R. Hu, and X. B. Luo, Opt. Express **28**, 875–885 (2020).
[19]A. V. Zayats, I. I. Smolyaninov, and A. A. Maradudin, Rev. Phys. **408**, 131–314 (2005).
[20]L. P. Wang and Z. M. Zhang, Appl. Phys. Lett. **100**, 063902 (2012).
[21]X. Li, G. Haberfehlner, U. Hohenester, O. Stéphan, G. Kothleitner, and M. Kociak, Science **371**, 1364–1367 (2021).
[22]M. Kaliteevski, I. Iorsh, S. Brand, R. A. Abram, J. M. Chamberlain, A. V. Kavokin, and I. A. Shelykh, Phys. Rev. B **76**, 165415 (2007).
[23]S. Maruyama, T. Kashiwa, H. Yugami, and M. Esashi, Appl. Phys. Lett. **79**, 1393–1395 (2001).
[24]C. Y. Qin, Y. M. Guo, J. Y. Seo, Y. Shuai, J. Lee, and B. J. Lee, Opt. Express **28**, 15731–15743 (2020).
[25]N. Jeon, J. J. Hernandez, D. Rosenmann, S. K. Gray, A. B. F. Martinson, and J. J. Foley Iv, Adv. Energy Mater. **8**, 1801035 (2018).
[26]R. Hu, S. Iwamoto, L. Feng, S. Ju, S. Hu, M. Ohnishi, N. Nagai, K. Hirakawa, and J. Shiomi, Phys. Rev. X **10**, 021050 (2020).
[27]N. Nguyen-Huu, Y. B. Chen, and Y. L. Lo, Opt. Express **20**, 5882–5890 (2012).
[28]M. G. Moharam, E. B. Grann, D. A. Pommet, and T. K. Gaylord, J. Opt. Soc. Am. A **12**, 1068–1076 (1995).
[29]Z. J. Zhang, K. Park, and B. J. Lee, Opt. Express **19**, 16375–16389 (2011).
[30]P. Lalanne, J. Opt. Soc. Am. A **14**, 1592–1598 (1997).
[31]R. Hu, J. Song, Y. Liu, W. Xi, Y. Zhao, X. Yu, Q. Cheng, G. Tao, and X. Luo, Nano Energy **72**, 104687 (2020).
[32]T. Ueno, T. D. Rhone, Z. Hou, T. Mizoguchi, and K. Tsuda, Mater. Discov. **4**, 18–21 (2016).
[33]W. Shockley and H. J. Queisser, J. Appl. Phys. **32**, 510–519 (1961).
[34]M. E. Nell and A. M. Barnett, IEEE Trans. Electron Devices **34**, 257–266 (1987).
[35]L. G. Ferguson and L. M. Fraas, Sol. Energy Mater. Sol. Cells **39**, 11–18 (1995).
[36]M. A. Green, *Solar Cells: Operating Principles, Technology, and System Applications* (Prentice Hall, 1982).
[37]S. Hassan, C. F. Doiron, and G. V. Naik, Appl. Phys. Lett. **116**, 023903 (2020).
[38]L. P. Wang and Z. M. Zhang, Opt. Express **19**, A126–A135 (2011).
[39]W.-W. Zhang, H. Qi, Y.-M. Yin, and Y.-T. Ren, Opt. Commun. **479**, 126416 (2021).
[40]T. Li, S.-M. Wang, H. Liu, J.-Q. Li, F.-M. Wang, S.-N. Zhu, and X. Zhang, J. Appl. Phys. **103**, 023104 (2008).